Probing interplay of light momentum and fluid mechanics in two-layer liquids

Gopal Verma [1,2,*] Ashwini Kumar [3] Sapna Soni,[2] Kapil Yadav,[2] and Wei Li [1,*]
[1]*GPL Photonics Laboratory, State Key Laboratory of Luminescence and Applications, Changchun Institute of Optics, Fine Mechanics and Physics, Chinese Academy of Sciences, Changchun, Jilin 130033, People's Republic of China*
[2]*Gopal Photonics Research Laboratory, Basti, Pandari Mishra, Amari Bazar 272155, (U.P.), India*
[3]*Dr. Rammanohar Lohia Avadh University, Ayodhya 224001, Uttar Pradesh, India*

(Received 10 June 2023; accepted 14 February 2024; published 8 March 2024)

We present an experimental setup that utilizes a pump-probe laser configuration to investigate the interplay between light momentum and fluid mechanics in a two-layer liquid system. By inducing a nanometric bulge on the upper liquid layer, we observe the emergence of a transient bulge on the liquid-liquid interface propelled by viscous stress towards the liquid with a higher refractive index. Through the integration of non-invasive measurements and extensive numerical simulations, we successfully validate our experimental findings and elucidate the intricate interplay between light momentum theories [Minkowski, Math. Phys. Klasse **1908**, 53 (1908); M. Abraham, Rend. Circ. Mat. Palermo **28**, 1 (1909)] and fluid mechanics. Importantly, we demonstrate that the transient deformation height can serve as a valuable indicator of surface tension and viscosity, enabling precise nanoscale manipulation and holding great potential for advancements in sensors, actuators, and optical devices. The profound insights gained from this study offer significant promise for the advancement of microfluidics and optofluidics, driving progress in these fields.

DOI: 10.1103/PhysRevFluids.9.034801

I. INTRODUCTION

The transfer of momentum from photons to a dielectric surface exposed to electromagnetic radiation is explained by two conflicting theories proposed by Minkowski and Abraham [1,2]. Minkowski's theory suggests that there is an outward surface force that is proportional to the refractive index (n) resulting from the momentum transfer, whereas Abraham's theory predicts an inward force that is proportional to $1/n$. To test these theories [1–5], researchers have used radiation pressure-induced liquid interface deformation as a test bed [6–10]. These experiments have shed light on the debate, but more investigation is needed to fully understand the intriguing coupling of light momentum and fluid dynamics [11–13]. As stated in Ref. [11], it is asserted that the momentum of light in a dielectric medium is not a fundamental quantity; rather, it arises as a consequence of the interaction between optics and fluid mechanics. Therefore, one can anticipate that in a two-layer liquid system where only the interface is exposed to optical forces, these forces will cause deformation.

In this regard, many experiments have been conducted on air-liquid [6,7,9,14] and liquid-liquid interfaces [15–18]. However, it remains unclear how the deformation of the air-liquid interface in a two-layer liquid induces shear stress on the liquid-liquid interface, causing it to deform through

*Corresponding authors: gopal@gprl.org.in, weili1@ciomp.ac.cn

 ©2024 American Physical Society

the intriguing coupling of light momentum and fluid dynamics. Furthermore, for bilayer or even multilayer films, x-ray photon correlation spectroscopy (XPCS) is the only technique to measure interfacial dynamics directly by tuning the x-ray incident angle to excite x-ray standing waves and selectively enhance the illumination and thus scattering at a particular interface [19], However, the XPCS technique for liquids, including water and octanol, has drawbacks. It can be costly due to the specialized x-ray equipment that is required. Additionally, its flexibility may be limited, posing challenges in adapting to diverse liquid systems.

Optical techniques are preferred compared to other techniques for the measurement of viscosity and surface tension due to their cost-effective and noninvasive nature [7,12–14,20,21]. Unlike other techniques, optical methods do not require direct contact with the sample, which can alter the properties being measured. Additionally, optical methods provide high-precision measurements with minimal artifacts. Optical techniques also offer the advantage of being able to measure the properties of transparent and opaque liquids [21–23] without altering their properties.

In this paper, we introduce a noninvasive interferometric technique for investigating the interaction between light momentum and fluid dynamics [11–13]. By utilizing a pump laser, we induce deformation on the upper layer of a liquid-liquid interface through total internal reflection. This method amplifies the radiation pressure by threefold compared to normal incidence, thereby minimizing the potential heating effects. Remarkably, our observations reveal the formation of a bulge (Minkowski momentum transfer) on both the upper air-liquid and liquid-liquid interfaces, highlighting the intriguing coupling between light momentum and fluid dynamics. Through our technique, we were able to characterize the surface tension and viscosity without the need for direct exposure to light, resulting in minimal artifact-induced measurements. Furthermore, one can extend this approach to a multilayer liquid interface, showcasing its potential in the development of new sensors, actuators, and optical devices.

II. EXPERIMENTAL SETUP AND METHODS

In our experimental setup, the liquid under investigation was placed inside a spherical concave glass container. The liquid height at the bottom and top is h_b and h_u, respectively, as shown in Fig. 1(a). Furthermore, the system has two-dimensional (2D) axisymmetry, and we have modeled the geometry in the simulation using the properties of 2D axisymmetry. A high-powered laser was used as the pump beam, directed towards the center of the top layer liquid to induce deformation in the liquid interface through nearly total internal reflection, which is about 44.76° for air-octanol interface. To achieve high-contrast circular fringes from both the air-liquid and liquid-liquid interfaces, we employed an interferometric technique, as illustrated in Fig. 1. In order to simultaneously measure the deformation on both interfaces, we utilized a beam splitter to split the beam into two paths. The first part shines from the top, where we used a reference spherical concave glass. This glass not only helps us generate interference fringes from the reference glass surface and the air-liquid interface, but also acts as an enclosure to reduce air currents and other sources of noise. The second part shines from the bottom of the container so that the Fresnel reflection from the container and the liquid-liquid interface can interfere and form a good contrast of fringes. This method allowed us to precisely measure the deformation height without any contribution from the deformation at the air-liquid interface. This enabled us to obtain valuable information regarding the deformation characteristics of the interface in a controlled manner. The resulting interference produced stable and high-contrast circular fringes, reminiscent of Newton's rings, which were observed on the screen (as shown in the insets of Fig. 1). However, the fringes obtained from the liquid surface were stationary as a result of negligible natural evaporation. So, to make reference for the measurement, we have shined the pump beam to induce a deformation magnitude of the order of $(\lambda/4n_l)$, reducing its central thickness $h_u(t)$ and introducing a time-dependent relative phase shift $\Delta\phi(t)$ between the interfering beams. In our case, the probe laser was quasinormal (incidence angle $< 5^\circ$) to the interface, and one can obtain $\Delta\phi(t) \simeq \beta h_u(t)$, where $\beta = 4\pi n/\lambda$ is a constant that depends only on the refractive index n of the liquid and the probe wavelength λ. This enables

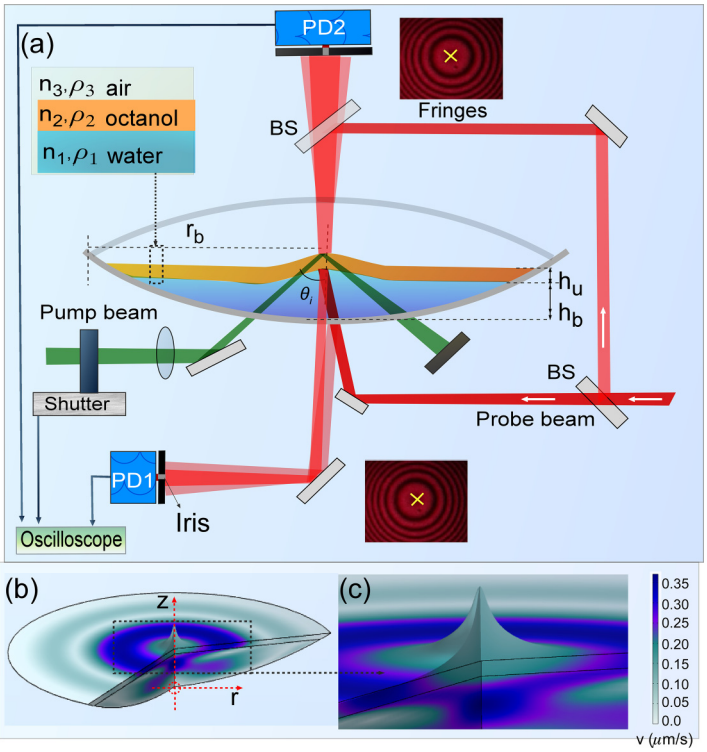

FIG. 1. (a) Schematics of the experimental setup. A collimated He-Ne probe beam ($P = 10$ mW, $\lambda = 632$ nm) is incident quasinormally from both above and below the liquid layers using a beam splitter (BS). This setup allows for simultaneous probing of the upper air-liquid and liquid-liquid interface deformations. A green pump beam with a power of $P_0 = 3$ W, $\lambda = 532$ nm, and a beam waist of $w = 155$ μm is focused on the air-liquid interface from below at an angle θ_i (partial reflection from the glass container and water-octanol interface not shown for clarity). The photodiodes PD1 and PD2 capture the intensity $I(t)$ of the central fringe simultaneously. The (b) bottom row figures and (c) their zoom display the numerically simulated deformation profile of liquid interfaces, where the color gradient represents the velocity, with the scale indicated in the legend.

us to calculate the deformation height of the nonevaporating liquid without requiring a reference surface [24,25], making the experimental setup compact and cost effective. See the Supplemental Material (SM) [26], Fig. S1, for more details. We investigated the air-octanol-water liquid system using a pump-probe laser beam. By carefully aligning the laser beam to satisfy the condition of total internal reflection on the air-octanol interface, which occurs at an approximate angle of 44.76°, we were able to observe intriguing phenomena, as shown in Figs. 2 and 3.

III. THEORY: DYNAMICS OF INTERFACE DEFORMATIONS

The theoretical description of small-amplitude deformations of free surfaces induced by radiation pressure has already been established for semi-infinite transparent liquid layers and experimentally investigated [8,23]. The discontinuity in light momentum at the air-water (AW) interface results in radiation pressure, capable of forming a stationary bulge on the interface. This pressure is counteracted by both buoyancy and Laplace pressure at the interface, as detailed in the work in Ref. [8]. In essence, this description is derived from the linearized unsteady Stokes equations, mass conservation, and stress balance at the free surface. For small-amplitude deformations $h(r, t)$,

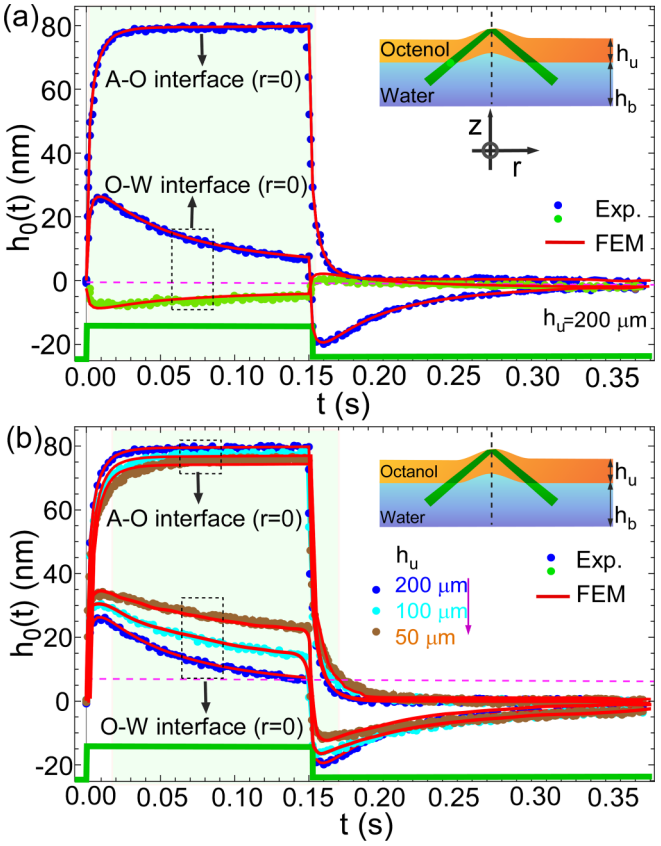

FIG. 2. The time-resolved deformation heights $h_0(t)$ of the air-octanol and octanol-water interfaces under total internal reflection (TIR) excitation are shown. In (a), the interface dynamics are depicted for both interfaces, with $h_u = 200$ μm and $h_b = 1.5$ mm. In (b), the interface dynamics are shown for three heights. The insets in the figures illustrate the direction of deformation and the path of the pump laser. The red solid lines represent the numerically simulated data obtained using the finite-element method (FEM)-based software, COMSOL MULTIPHYSICS.

characterized by $h/w \ll 1$ (where w is pump laser beam), the stress balance at the interface can be expressed as follows:

$$(\rho_i - \rho_t)gh(r,t) - \frac{\gamma}{r}\frac{\partial}{\partial r}[rh(r,t)] - 2\eta\frac{\partial v_z}{\partial z}(r,t) = \Pi(\theta_i, r), \tag{1}$$

where $v_z(r,t)$ represents the vertical velocity of the liquid, describing the evolution of the surface deformation using the approximation $h(r,t) = \int_0^t v_z(r,t)\,dt$ and

$$\Pi(\theta_i, r) = \frac{n_i I(r)}{c}\cos^2\theta_i\left[1 + R - \frac{\tan\theta_i}{\tan\theta_t}T\right],$$

where c represents the speed of light. The indexes i and t, respectively, refer to incident and transmitted ray, and hence for the total internal reflection (TIR) on an air-octanol interface, ρ_i and ρ_t densities of the octanol and air, respectively. $n_i = n_2$ and $n_t = n_3$ denote the refractive indices of the octanol and air. The laser intensity is given by $I(r) = 2P_0/\pi w^2 \exp(-2r^2/w^2)$, where P_0 is the total power and w is the beam waist at the focus. Additionally, γ and g represent the interfacial surface tension of the liquid and gravitational acceleration, respectively. θ_i and θ_t represent the angles of

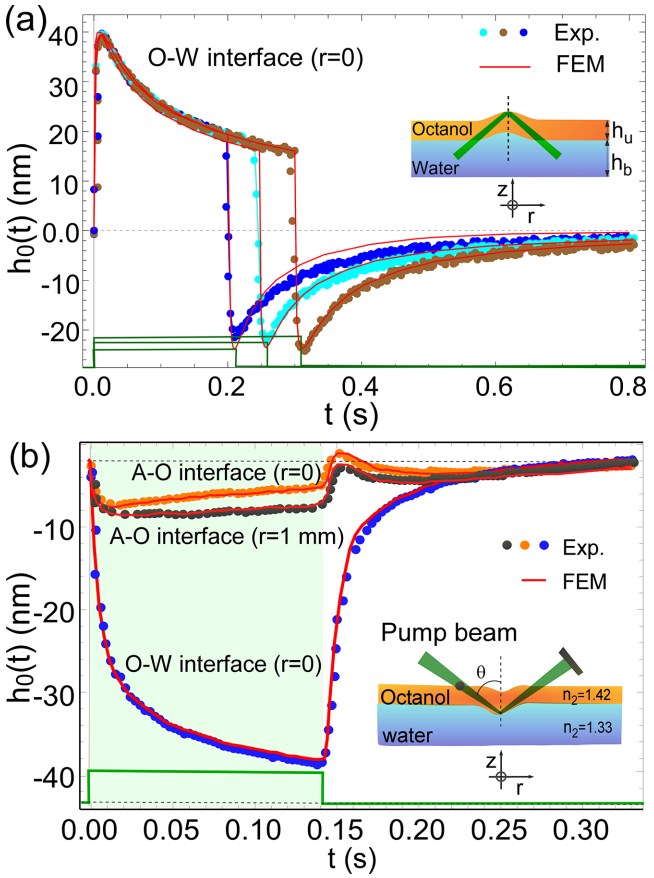

FIG. 3. (a) The transient deformation height $h_0(t)$ of the octanol-water interface is measured for three different exposures. (b) When the pump beam shines from the top and TIR occurs at the octanol-water interface, the transient $h_0(t)$ is recorded for both the air-octanol and octanol-water interfaces.

incidence and transmission, respectively. R and T correspond to the reflectance and transmittance at the interfaces.

Finally, we find the expected dynamics of the interface deformation on the beam axis $h(r=0,t)=h_0(t)$, and its relaxation after an exposure time t_0 [23],

$$h_0(t \leqslant t_0) = \frac{\Pi_0}{4\gamma k_c^2}\int_0^\infty \frac{\exp\left(-\tilde{k}^2/8\right)}{\mathrm{Bo}+\tilde{k}^2}\{1-\exp[-\Omega(\tilde{k})t]\}\tilde{k}\,\mathrm{d}\tilde{k},$$
$$h_0(t \geqslant t_0) = \frac{\Pi_0}{4\gamma k_c^2}\int_0^\infty \frac{\exp\left(-\tilde{k}^2/8\right)}{\mathrm{Bo}+\tilde{k}^2}\{1-\exp[-\Omega(\tilde{k})t_0]\}\exp[-\Omega(\tilde{k})t]\tilde{k}\,\mathrm{d}\tilde{k}, \quad (2)$$

where $\tilde{k}=k/k_c$ is the dimensionless wave number, with characteristic wave number as $k_c=1/w$, and $\Omega(\tilde{k})$ is the rate of evolution of the overdamped mode $\tilde{k}$. Π_0 is the amplitude of the radiation pressure on the beam axis. The corresponding optical Bond number is $B_o=(w/l_c)^2$, where $l_c=\sqrt{\gamma/\Delta\rho g}$, and where $\Delta\rho=|\rho_i-\rho_t|$ represents the difference in density. In the thick-layer case considered above ($h_{u,b}/w \gg 1$), one has

$$\Omega(\tilde{k}) = \frac{1}{\tau}\tilde{k}\frac{(1+\mathrm{Bo}/\tilde{k}^2)}{1+\mathrm{Bo}},$$

TABLE I. Liquids parameters used in simulations and measured experimentally.

Parameter	Unit	Simulation	Measured value
$R_{\text{water,octanol}}$		1.33,1.42	
$\rho_{\text{water,octanol}}$	kg/m^3	998, 865	
$\gamma_{\text{water,octanol}}$	N/m	0.071, 0.0285	0.070, 0.0281
$\eta_{\text{water,octanol}}$	Pa s	0.0010, 0.0071	0.0012, 0.0069

which allows one to define a characteristic damping time (τ) associated to the mode k_c,

$$\tau = \frac{2\eta}{\gamma k_c}(1+\text{Bo})^{-1} = \frac{2\eta w}{\gamma}(1+\text{Bo})^{-1}. \tag{3}$$

We have used Eqs. (2) and (3) above to compare the experimental as well as simulation data (see more details about the derivation of Eqs. (2) and (3) in the SM [26]). To ensure optimal conditions, such as avoiding the meniscus effect from the container wall and ensuring $h_{u,b}/w \gg 1$, we maintained the thickness of the liquid in the central region below 2 mm, with a typical diameter of approximately 15 mm.

Figure 2(a) shows the bulge height $h_0(t)$ for the pump power ($P_0 = 3$ W) in the TIR configuration ($\theta_i = 45^\circ$), considering three different values of the top-layer octanol thickness. The bulge height was averaged over three shots of the shutter opening for a given power. The presence of a bulge on the air-octanol (AO) interface is in accordance with Minkowski's momentum and is also consistent with prior findings [6–9]. Remarkably, we also noted that the water-octanol interface underwent deformation, initially forming a pronounced bulge. This transient bulge showed a clear orientation directed toward the octanol layer, which has a higher refractive index (1.42) in contrast to water (1.33). This observation underscores the existence of a robust connection between radiation pressure and interface deformation, which holds in both transient and steady states. However, it is important to note that the mere presence of a bulge or dip does not, by itself, provide conclusive evidence regarding the nature of light's momentum. As demonstrated in [11–13], fluid flow and geometric factors also play pivotal roles. Furthermore, we calculated the deformation on the water-octanol interface where the pump laser entered and exited, which was less than 6 nm and not shown in Fig. 2(b) to avoid the complexity.

First, we validated our data [Fig. 2(a)] with Eqs. (2) and (3). According to these equations, the fit of the growing deformation gives the amplitude $\Pi_0 w^2/4\gamma$, the timescale τ, and the Bo number value. From the amplitude, we get γ when n is known. From the measured timescale τ_{exp} (here corresponding to τ), we determine the viscous velocity γ/η and then η. Taking into account the height resolution of ± 1 nm, on the one hand, and the relative error $d\tau_{\text{exp}}/\tau_{\text{exp}} = 1\%$ deduced from the standard deviation, on the other hand, we finally find $\gamma = (24 \pm 2)$ mNm^{-1} and $\eta = (7.1 \pm 0.05)$ mPa s for the air-octanol interface, in very good agreement with the literature [27] ($\gamma = 24.8$ mNm^{-1} and $\eta = 7.10$ mPa s at $20\,^\circ$C). The dynamics of deformation predicted for the thick-layer case ($h_{u,b}/w \gg 1$) is thus quantitatively retrieved experimentally (see the SM, Fig. S1, for more details [26]). We have previously studied [23] a scaling analysis that takes into account radiation pressure, viscosity, and film thickness and found that the dynamics of the thin film also depends upon film thickness. We also analyzed the fringes obtained from light reflection at the bottom glass and the liquid-liquid (water-octanol) interface using the same procedure. In the final results for both interfaces, we summarized the parameters used in the simulation, incorporating data from the literature [27], as well as our measured data, in Table I.

The variation of exposure time for a pump laser is a crucial factor to consider in the study of liquid-liquid interfaces. By adjusting the exposure time, one can observe and analyze the transient dynamics occurring at the interface between water and ethanol. One could explore experimental setups involving higher viscosity ratios by utilizing viscous mixtures such as glucose-water with

hexadecane, or glucose-water with toluene, combined with suitable surfactants. By employing such experimental conditions, one can investigate the effects and behaviors of fluids with substantially different viscosities, providing valuable insights into various phenomena and processes [see Fig. 3(a)].

Furthermore, if we shine a pump laser from the top onto the liquid ($n_i = n_2$ and $n_t = n_1$), satisfying the total internal reflection (TIR) angle condition on the liquid-liquid interface, the momentum discontinuity generates radiation pressure, deforming the liquid-liquid interface and forming a dimple (in agreement with Minkowski momentum).

Additionally, a transient dimple forms on the air-liquid (octanol) interface due to viscous stress, as shown in Fig. 3. Transient dimples on the air-liquid interface find applications in microfluidics and surface-tension-based devices, offering diverse opportunities for advancement in different fields [28].

IV. FINITE-ELEMENT METHOD (FEM)-BASED NUMERICAL SIMULATION

In order to validate our experimental data and ensure reliable predictions across different conditions, we utilize the FEM-based software COMSOL MULTIPHYSICS. This computational approach empowers us to simulate and analyze the system's behavior with high precision. By employing this methodology, we can unravel the intricate interplay between light momentum and fluid dynamics at the interface, gaining valuable insights into their interaction [7,12,22]. By modeling a two-layer liquid system and solving the Navier-Stokes equation with appropriate boundary conditions, we investigate the effect of the transient deformation profile of the liquid interface. The calculations involve considering the effects of radiation pressure on the surface displacement, utilizing the Laminar two-phase flow, moving mesh module, for solving the incompressible flow equations,

$$\rho\frac{\partial v}{\partial t} + \rho(v\nabla)v = -\nabla P + \eta\nabla^2 v + F,$$

where v describes the flow velocity, P is the pressure, ρ is the fluid density, and η is the dynamic viscosity. The model was built in two-dimensional (2D) axisymmetric geometry, as shown in Fig. 4(a).

The external pressure and surface tension act on the boundary condition of the free surface. However, surface tension on a liquid-liquid interface is applied through a boundary condition using the feature of a fluid-fluid interface. For the general angle of incident $P(\theta_i, r) = f(\theta_i)2n_i(n_i - n_t)I/c(n_i + n_t)$, where $f(\theta_i) = \cos^2\theta_i[1 + R - (\tan\theta_i/\tan\theta_t)T]$ and $I(r) = (2P_0/\pi w^2)\exp(-2r^2/w^2)$ is the intensity of incident light beam, θ_i and θ_t denote the angles of incidence and transmission, respectively. Free-surface and no-slip boundary conditions were applied at the air-liquid and substrate interfaces $v_r(z = h_b) = 0$ and the velocity is continuous at the liquid-liquid (water-octanol) interface. The gravity vector entered the force term as $\mathbf{F} = -\rho\mathbf{g}$, with $g = 9.8\ \mathrm{m/s^2}$ [7,12,22]. Realistic sample geometry was considered [Fig. 4(a)], with $r_b = 15$–20 mm and upper- and bottom-layer liquid thickness $h_u = 0.02$–1 mm and $h_b = 0.5$–1 mm, respectively. We have compared the experimental, theoretical, and FEM results and found good agreement. These results are presented in the SM, Fig. S2 [26].

Finding a visible light transparent liquid-liquid interface with water on top poses challenges including refractive index matching, chemical compatibility, and stability. Examples include the water-oil interface, such as water-chloroform [29], requiring careful consideration due to aesthetics. Our study employed FEM simulations for the water-chloroform interface, revealing a transient bulge formation on the water surface [Fig. 4(b)]. This observation confirms the coupling between light momentum and fluid dynamics, as mentioned previously.

The results of our study demonstrate a fascinating interplay between light momentum and fluid dynamics in a two-layer liquid system, as elucidated by our pump-probe laser setup. By applying the pump laser, we induce a nanometric bulge on the upper liquid layer. Interestingly, this induced bulge also triggers a transient bulge on the liquid-liquid interface due to the viscous stress exerted in the

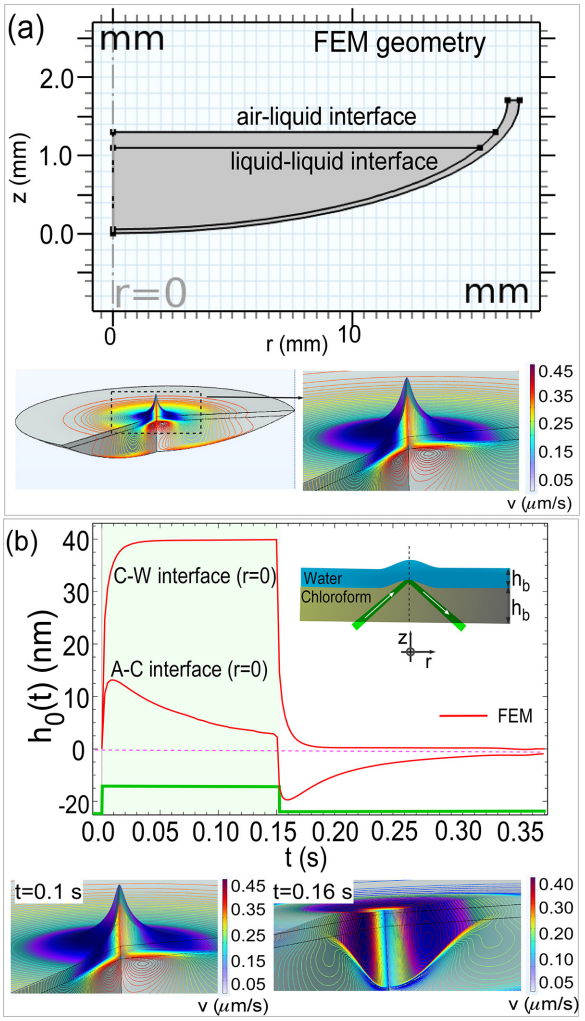

FIG. 4. (a) A 2D-axisymmetric geometry is employed in the FEM simulation. (b) The transient deformation height $h_0(t)$ is plotted for both the air-water and water-chloroform interfaces. In both cases [(a) and (b)], the bottom row shows the deformed interface profile along with velocity contour lines.

direction of the higher refractive index liquid. This behavior is contrary to the expected Minkowski momentum transfer, adding a different aspect to the observed coupling phenomenon.

Importantly, our technique offers a noninvasive approach to investigating the surface tension and viscosity of multilayer liquid systems. Unlike traditional methods that require direct exposure of the pump laser, our approach eliminates the need for such high-power laser exposure, minimizing any potential artifacts that may arise from light-induced effects [12,14,22]. This is a significant advantage as it allows for a more accurate characterization of the system without introducing unwanted perturbations.

To support and validate our experimental findings, we conducted numerical simulations using realistic experimental parameters. The agreement between the experimental results and the simulations further strengthens our conclusions and provides a comprehensive understanding of the underlying physics governing the coupling of light momentum and fluid dynamics in a two-layer liquid system. The implications of our study extend beyond fundamental research, offering different

possibilities for a wide range of applications. The ability to investigate surface tension and viscosity in two-layer liquid systems [28,30] without direct exposure to the pump laser opens avenues for the development of innovative sensors, actuators, and optical devices [28]. By leveraging the coupling phenomenon observed in our study, future technologies can be designed with enhanced performance and functionality [31,32].

V. CONCLUSION

In conclusion, our study sheds light on the intricate relationship between light momentum and fluid dynamics in two-layer liquid systems. Through a noninvasive technique and rigorous experimental validation, we have gained insights into the coupling mechanism and its potential applications. The control of the shape of the free surface [33] and liquid-liquid interface holds significance in engineering applications in tunable optofluidic [34] elements. Supported by realistic numerical simulations, our findings offer different possibilities for the development of sensors, actuators, and optical devices in optofluidics [32,35] and reconfigurable optics [31,32].

ACKNOWLEDGMENTS

We thank Gyanendra Yadav for insightful discussions. This work was supported by the National Natural Science Foundation of China (Grants No. 62134009 and No. 62121005), and the Innovation Grant of Changchun Institute of Optics, Fine Mechanics and Physics (CIOMP).

[1] H. Minkowski, Die grundgleichungen für die elektromagnetischen vorgänge in bewegten körpern, Nachrichten von der Gesellschaft der Wissenschaften zu Göttingen, Math. Phys. Klasse **1908**, 53 (1908).
[2] M. Abraham, Zur elektrodynamik bewegter körper, Rend. Circ. Mat. Palermo **28**, 1 (1909).
[3] S. M. Barnett, Resolution of the Abraham-Minkowski dilemma, Phys. Rev. Lett. **104**, 070401 (2010).
[4] R. Peierls, The momentum of light in a refracting medium, Proc. R. Soc. London, Ser. A **347**, 475 (1976).
[5] R. N. C. Pfeifer, T. A. Nieminen, N. R. Heckenberg, and H. Rubinsztein-Dunlop, Colloquium: Momentum of an electromagnetic wave in dielectric media, Rev. Mod. Phys. **79**, 1197 (2007).
[6] A. Ashkin and J. M. Dziedzic, Radiation pressure on a free liquid surface, Phys. Rev. Lett. **30**, 139 (1973).
[7] N. G. C. Astrath, L. C. Malacarne, M. L. Baesso, G. V. B. Lukasievicz, and S. E. Bialkowski, Unravelling the effects of radiation forces in water, Nat. Commun. **5**, 4363 (2014).
[8] G. Verma and K. P. Singh, Universal long-range nanometric bending of water by light, Phys. Rev. Lett. **115**, 143902 (2015).
[9] G. Verma, K. Chaudhary, and K. P. Singh, Nanomechanical effects of light unveil photons momentum in medium, Sci. Rep. **7**, 42554 (2017).
[10] L. Zhang, W. She, N. Peng, and U. Leonhardt, Experimental evidence for Abraham pressure of light, New J. Phys. **17**, 053035 (2015).
[11] U. Leonhardt, Abraham and Minkowski momenta in the optically induced motion of fluids, Phys. Rev. A **90**, 033801 (2014).
[12] G. Verma, G. Yadav, and W. Li, Thin-film dynamics unveils interplay between light momentum and fluid mechanics, Opt. Lett. **48**, 123 (2023).
[13] G. Verma, V. Kumar, and W. Li, Revealing light momentum in dielectric media through standing-wave radiation pressure, Phys. Rev. A **108**, 043514 (2023).
[14] K. Sakai and Y. Yamamoto, Electric field tweezers for characterization of liquid surface, Appl. Phys. Lett. **89**, 211911 (2006).
[15] N. Bertin, H. Chraïbi, R. Wunenburger, J.-P. Delville, and E. Brasselet, Universal morphologies of fluid interfaces deformed by the radiation pressure of acoustic or electromagnetic waves, Phys. Rev. Lett. **109**, 244304 (2012).

[16] A. Casner and J.-P. Delville, Laser-induced hydrodynamic instability of fluid interfaces, Phys. Rev. Lett. **90**, 144503 (2003).
[17] E. Brasselet, R. Wunenburger, and J.-P. Delville, Liquid optical fibers with a multistable core actuated by light radiation pressure, Phys. Rev. Lett. **101**, 014501 (2008).
[18] Z. Jiang, H. Kim, S. G. J. Mochrie, L. B. Lurio, and S. K. Sinha, Surface and interfacial dynamics of polymeric bilayer films, Phys. Rev. E **74**, 011603 (2006).
[19] C. Gutt, T. Ghaderi, V. Chamard, A. Madsen, T. Seydel, M. Tolan, M. Sprung, G. Grübel, and S. K. Sinha, Observation of heterodyne mixing in surface x-ray photon correlation spectroscopy experiments, Phys. Rev. Lett. **91**, 076104 (2003).
[20] G. Verma and K. P. Singh, Time-resolved interference unveils nanoscale surface dynamics in evaporating sessile droplet, Appl. Phys. Lett. **104**, 244106 (2014).
[21] G. Verma, G. Yadav, C. S. Saraj, L. Li, N. Miljkovic, J. P. Delville, and W. Li, A versatile interferometric technique for probing the thermophysical properties of complex fluids, Light Sci. Appl. **11**, 115 (2022).
[22] O. A. Capeloto, V. S. Zanuto, L. C. Malacarne, M. L. Baesso, G. V. B. Lukasievicz, S. E. Bialkowski, and N. G. C. Astrath, Quantitative assessment of radiation force effect at the dielectric air-liquid interface, Sci. Rep. **6**, 20515 (2016).
[23] G. Verma, H. Chesneau, H. Chraibi, U. Delabre, R. Wunenburger, and J.-P. Delville, Contactless thin-film rheology unveiled by laser-induced nanoscale interface dynamics, Soft Matter **16**, 7904 (2020).
[24] G. Verma, M. Pandey, and K. P. Singh, Interferometric technique for nanoscale dynamics of fluid drops on arbitrary substrates, J. Appl. Phys. **118**, 035306 (2015).
[25] P. Munjal and K. P. Singh, A single-lens universal interferometer: Towards a class of frugal optical devices, Appl. Phys. Lett. **115**, 111102 (2019).
[26] See the Supplemental Material at http://link.aps.org/supplemental/10.1103/PhysRevFluids.9.034801 for the calculation of the deformation height in the case of a nonevaporating drop, as illustrated in Figs. (2)–(4). No reference surface is required, thus making the experimental setup compact and cost effective, as demonstrated in Refs. [24,25]. The dynamics of deformation predicted for the thick-layer case ($h_u, h_b/w \gg 1$) are thus quantitatively retrieved experimentally, as reported in Ref. [23].
[27] S. Mitani and K. Sakai, Measurement of ultralow interfacial tension with a laser interface manipulation technique, Phys. Rev. E **66**, 031604 (2002).
[28] K. Wei, H. Huang, Q. Wang, and Y. Zhao, Focus-tunable liquid lens with an aspherical membrane for improved central and peripheral resolutions at high diopters, Opt. Express **24**, 3929 (2016).
[29] B. Issenmann, A. Nicolas, R. Wunenburger, S. Manneville, and J.-P. Delville, Deformation of acoustically transparent fluid interfaces by the acoustic radiation pressure, Europhys. Lett. **83**, 34002 (2008).
[30] Y. Niño, R. Caballero, and L. Reyes, Mixing and interface dynamics in a two-layer stratified fluid due to surface shear stress, J. Hydraul. Res. **41**, 609 (2003).
[31] B. J. Monat, C. Domachuk, and P. Eggleton, Integrated optofluidics: A new river of light, Nat. Photon. **1**, 106 (2007).
[32] C. Psaltis, D. Quake, and S. R. Yang, Developing optofluidic technology through the fusion of microfluidics and optics, Nature (London) **442**, 381 (2006).
[33] G. Verma, C. S. Saraj, G. Yadav, S. C. Singh, and C. Guo, Generalized emptying criteria for finite-length capillary, Phys. Rev. Fluids **5**, 112201(R) (2020).
[34] G. Verma, G. Yadav, Y. Shi, L.-M. Zhou, C.-W. Qiu, and W. Li, Tunable optofluidic curvature for micromanipulation, Laser Photon. Rev. **18**, 2300539 (2023).
[35] A. Dogariu, S. Sukhov, and J. Saenz, Optically induced negative forces, Nat. Photon. **7**, 24 (2013).